NASA CONTRACTOR REPORT

NASA CR-2445

NASA CR-2445

EXPERIMENTAL EVALUATION OF STRESSES IN SPHERICALLY HOLLOW BALLS

by L. J. Nypan

Prepared by
CALIFORNIA STATE UNIVERSITY
Northridge, Calif. 91324
for Lewis Research Center

NATIONAL AERONAUTICS AND SPACE ADMINISTRATION • WASHINGTON, D. C. • AUGUST 1974

1. Report No.	2. Government Accession No.	3. Recipient's Catalog No.
NASA CR-2445		

4. Title and Subtitle	5. Report Date
EXPERIMENTAL EVALUATION OF STRESSES IN SPHERICALLY HOLLOW BALLS	August 1974
	6. Performing Organization Code

7. Author(s)	8. Performing Organization Report No.
L. J. Nypan	None
	10. Work Unit No.

9. Performing Organization Name and Address	11. Contract or Grant No.
California State University 18111 Nordhoff Street Northridge, California 91324	NGL 05-062-002
	13. Type of Report and Period Covered
12. Sponsoring Agency Name and Address	Contractor Report
National Aeronautics and Space Administration Washington, D. C. 20546	14. Sponsoring Agency Code

15. Supplementary Notes

Final Report. Project Manager, Harold H. Coe, Fluid System Components Division, NASA Lewis Research Center, Cleveland, Ohio

16. Abstract

An experimental stress analysis was undertaken to evaluate stresses within spherically hollow bearing balls proportioned for 40, 50, and 60% mass reductions. Strain gage rosettes were used to determine principal strains and stresses in the steel ball models statically loaded in various orientations. Dimensionless results are reported for the balls under flat plate contact loads. Similitude considerations permit these results to be applied to calculate stresses in hollow bearing balls proportioned to these mass reductions.

17. Key Words (Suggested by Author(s))	18. Distribution Statement
Hollow balls; Ball bearings; Stress analysis	Unclassified - unlimited Category 15

19. Security Classif. (of this report)	20. Security Classif. (of this page)	21. No. of Pages	22. Price*
Unclassified	Unclassified	48	$3.25

* For sale by the National Technical Information Service, Springfield, Virginia 22151

TABLE OF CONTENTS

LIST OF FIGURES

LIST OF TABLES

I. SUMMARY

An experimental stress analysis was undertaken to evaluate stresses within spherically hollow bearing balls proportioned for 40, 50, and 60% mass reductions. Strain gage rosettes were used to determine principal strains and stresses in the steel ball models statically loaded in various orientations.

Dimensionless results are reported for the balls under flat plate contact loads. Similitude considerations permit these results to be applied to calculate stresses in hollow bearing balls proportioned to these mass reductions.

II. INTRODUCTION

Aircraft gas turbine engines currently operate in a speed range of 1.5 to 2 million DN (bearing bore in mm times shaft speed in rpm). It is estimated that engine designs of the next decade will require bearings to operate at DN values of 3 to 4 million. In this DN range, the reduction in bearing fatigue life due to the high centrifugal forces developed between the rolling elements and outer race becomes prohibitive.(1)[1]

To solve the problems of reduced fatigue life in high-speed ball bearings various methods of reducing centrifugal force have been proposed. One of these is to reduce the ball mass by welding forged hollow hemispheres and finishing the spheres in a manner similar to solid balls. Full-scale bearing tests with spherically hollow ball bearings have demonstrated that operation is possible.(2) Fracture of spherically hollow balls has also been experienced during the operation of the full-scale bearings.

Analysis of the failures experienced, and the effect of changes in ball characteristics and configuration on high speed operation has been handicapped by the difficulty of application of theory to predict stresses existing in the balls under bearing loads and centrifugal forces applied at various locations on the balls. It is the object of this investigation to provide this stress information by determining experimentally the surface stresses in spherically hollow balls through the use of oversize ball models of sufficient size to instrument with strain gage rosettes so that conventional experimental stress analysis techniques may be employed to

[1]Numbers in parentheses designate references at end of report.

obtain this information.

Strain gage techniques have been used to determine the surface stress distribution in spherically hollow balls proportioned for mass reductions of 40, 50 and 60 per cent.

III. MODELS

Actual bearing balls dynamically loaded in a full scale ball bearing would be difficult to instrument for experimental stress analysis. The models used in this study were selected for ease of fabrication and instrumentation. Hemispheres were turned from mild steel bar stock with a radius cutting tool to a 63.5 (2.5 in) radius spherical contour, and turned to a spherical internal radius calculated to provide the desired mass reduction of 40, 50 and 60 per cent. The hemispheres were strain gaged inside and out with internal leads brought out through a 7 mm (0.27 in) hole in the hemisphere opposite the gages. Figure 1 gives model dimensions. The mild steel materials simplified metal cutting. Its lack of hardness was not a problem as care was taken to insure that strains were always within the elastic range. The 127 mm (5 in) model size seemed to be compatible with available 1 mm gage length strain gage rosettes and proved easy to position and load in a unversal testing machine. TML ZFRA-1 (1 mm gage length) 45^{o} strain gage rosettes were mounted on the models in locations shown in Figure 2. The hemispheres were bonded with epoxy adhesive. Evaluation of strain gage data seemed to indicate that the bond line transmitted forces and moments sufficiently well that data from rosettes nearest the bond line was indistinguishable from the data of rosettes more distant from the bond line.

The rosettes were mounted with one strain gage of each rosette aligned along a common great circle of one hemisphere over a quadrant. Other strain gages on the rosette backing were then automatically aligned at 45^{o} and 90^{o} to the great circle. A line of rosettes was thus established along a great circle on the interior and exterior of the model.

Loads were applied statically at four load points by repositioning the model each time after the rosette indications had been recorded. As seen in Figure 2 these load points were midway between the external rosettes. Loads were carefully limited to protect the models while still providing a measurable strain gage response. The models were positioned by eye to provide load over the desired load point marked on the outside of the model. Figure 3 shows the models used, and Figure 4 shows a model positioned in the testing machine. Strains proved to be very sensitive to load orientation for the most highly loaded gages.

IV. INSTRUMENTATION

A Baldwin-Lima-Hamilton Model 120 strain indicator was used to power a Wheatstone strain gage bridge incorporating a temperature compensating strain gage as one of the bridge arms. The strain indicator scope output jack was used to drive a Mosely 7000 A XY plotter to amplify and record the strain indicator signal. The recorder pen deflection was found to be linear with strain indicator unbalance, and the recorder could be calibrated so that 25.4 mm (1 in) of pen deflection corresponded to 100 micro mm/mm (100 micro in/in) of strain indicator unbalance. The recorder then could provide a $\pm$ 190.5 mm ($\pm$ 7.5 in) pen deflection and record for a $\pm$ 750 micro m/m ($\pm$ 750 micro in/in) strain unbalance of the bridge by the active strain gage. Standard commercial Baldwin-Lima Hamilton and Budd switch and balance units were used to switch individual gages of the rosettes to the strain indicator and to provide initial zero adjustment for each gage. As each gage was switched to the strain indicator and the gage unbalance deflected the pen in the "X" direction a record was made by deflecting the pen 2.54 mm (.1 in) in the "Y" direction.

These records could later be read to .25 mm (.01 in) so that the resolution of the recording system was 1 micro m/m (1 micro in/in). Successive records made over the gages of a model while the model was undisturbed in the testing machine at constant load indicated an overall repeatability of $\pm$ 5 micro mm/mm ($\pm$ 5 micro in/in) for the overall instrumentation system under this condition.

When a supposedly identical series of data records were taken on different days deviations of $\pm$ 60 micro m/m ($\pm$ 60 micro in/in) could occasionally

be detected. These were attributed to difficulty in obtaining identical model-load orientation, and strain gage and adhesive hysteresis effects superimposed on the above switch contact-strain indicator-recorder variations. A technique of averaging data was successful in reducing the effect of this variation.

Figure 5 is a circuit diagram of the instrumentation. Figure 6 is an overall view of the physical arrangement of the apparatus.

V. RESULTS AND DISCUSSION

Strains read from the recorder charts were used to compute principal strains and stresses for each rosette. These are given in Tables 2, 3, and 4.

In these tables epsilon A is the latitudinal strain along a great circle of the model, read from the output of a strain gage mounted along the great circle. Epsilon B is the strain 45^{o} to epsilon A, and epsilon C is the longitudinal strain, read from the strain gage mounted at 90^{o} to epsilon A. The data reads from the top down as the rosette closest to the symmetry point of the strain gaged hemisphere downward toward the joint of the sphere.

Epsilon 1 and epsilon 2 are the computed principal strains. All strains are given in micro m/m (micro in/in) with epsilon 1 always being the algebraically larger (most positive) of the principal strains.

The principal strains were calculated from the measured strains using equations from Dally and Riley.[3]

$$\epsilon_{1,2} = \frac{1}{2}(\epsilon_A + \epsilon_C) \pm \frac{1}{2}\sqrt{(\epsilon_A - \epsilon_C)^2 + (2\epsilon_B - \epsilon_A - \epsilon_C)^2} \qquad (1)$$

Principal stresses were then computed from:

$$\sigma_1 = \frac{E}{1 - \nu^2}(\epsilon_1 + \nu\epsilon_2) \qquad (2)$$

$$\sigma_2 = \frac{E}{1 - \nu^2}(\epsilon_2 + \nu\epsilon_1) \qquad (3)$$

with values for modulus of elasticity, E, of 207×10^9 N/m^2 (30×10^6 lb/in^2)

and a Poisson's ratio, ν, of 0.3 These were then used to detrmine dimensionless stress coefficients from:

$$K_1 = \frac{\sigma_1}{\frac{P}{\pi R_o^2}} \tag{4}$$

$$K_2 = \frac{\sigma_2}{\frac{P}{\pi R_o^2}} \tag{5}$$

where: R_o = the outer radius of the model

P = the load required to produce the measured strain.

Loads used were limited to protect the models by observing the output of the gages and stopping the loading when a significant indication was observed. There was some uncertainty as to the adequacy of the epoxy joints in the models, however, the data obtained proved to be consistent when a number of measurements were averaged, and the loads reported in Tables 2, 3 and 4 were found adequate for the purposes of the study.

Five independent sets of data were obtained at each load location over a number of days. The model was removed from the universal test machine and repositioned for each data determination. The strain data measured from the chart records was analyzed by computing the mean values of the 5 determinations of ε_A, ε_B and ε_C; the deviation of each determination from the mean and the standard deviations of ε_A, ε_B, and ε_C. Deviations were scrutinized carefeully, and chart records reexamined where deviations were greater than 15 micro m/m. While this helped to eliminate large errors in observations, there were still standard deviations of up to 28 micro m/m

in measurements of 144 micro m/m magnitude. The largest variation occured where rosettes were almost directly below the load location, and are attributable to the great variation in dimensionless stress coefficient with angular orientation to the load, as may be seen in Figures 7, 8 & 9. In spite of large differences in independent data determinations for some rosettes the averaging of 5 data sets and use of all available data gave smooth curves that were consistent with the theory of elasticity series solution given by Golecki[4] and discussed in Section VI of this report.

While only 5 rosettes inside each model and 3 rosettes on the outside of the models were used, the model symmetry and the interlacing of the indicated stress coefficients for the load locations used permitted the curves of Figures 7, 8 and 9 to be drawn. Stress coefficients given in Tables 2, 3 and 4 were plotted separately for each load location and then transferred to a single sheet with the aid of a light table.

From Figure 7, 8 and 9 it may be seen that maximum stress coefficients are 43.1, 75.9 and 142.8 for the 40, 50 and 60% mass reduction balls. It would seem then that stresses in a 40% mass reduction ball will be 0.568 of those in a 50% mass reduction ball, while stresses in a 60% mass reduction ball will be 1.88 times those in a 50% mass reduction ball, all other things being equal. If centrifugal force is the principal loading factor on the balls a change from 50% to 40% mass reduction balls would increase load by 6/5 but reduce bending stresses by a factor of 0.682. Conversely going to a 60% mass reduction ball from a 50% mass reduction ball would reduce centrifugal force by 4/5, but increase stress by a factor of 1.5. Contact stresses will still be greatest for the 40% mass reduction case.

VI. COMPARISON WITH THEORY

Golecki [4] has given a theory of elasticity series solution for the state of stress in "The Sphere Weakened by a Concentric Inclusion of Different Elastic Properties Under Concentrated Loads". Pih and Vanderveldt [5] have shown that for spheres with ratios of internal to external diameter of .25 and .33, the series is oscillatory for radial distances greater than 0.5 times outer radius and actually diverges near the outer boundary. The series was found to converge for the interior surface stresses of spheres proportioned for 40, 50 and 60% mass reductions. It was necessary to compute and sum 40 terms of the series before the last term of the series became sufficiently small in the worst case. Table 5 gives the theoretical values of stress coefficients computed for the three balls at 10 degree increments in angle Θ, the angle from the applied force

The coefficients given by the elasticity solution were used to plot the curves of Figures 7, 8 and 9 on which the experimentally determined non-dimensional stress coefficients are superimposed. Agreement between the curves and elasticity solution appears to be good.

Rumbarger [6] reported the result of a finite element computer analysis of a hollow ball contacting a flat plate. His ball model had a diameter of 25.4 mm (1 in), a wall thickness of 2.03 mm (.08 in) and was loaded to 4,450 N (1000 lb). He reported calculated interior bending stresses of 304,800 N (150,000 psi) directly under the load and 34,500 N (5,000 psi) at 90° to the load. The radius ratio for this case was .84.

From this it may be inferred that the ball was proportioned to a 59.3% mass reduction and that dimensionless stress coefficients would be -117.8 and 3.9 at 0° and 90°. These compare with values of -138.1 and 3.09

interpolated between Golecki's series solutions for a 59.3% mass reduction ball. The values are of an appropriate magnitude, but do not agree as well as do the experimental results reported here. The reason for the lack of agreement between Rumbarger and Golecki is not clear.

VII. CONCLUSION

The stress distribution in spherically hollow balls proportioned for mass reductions of 40, 50 and 60 per cent has been determined. A 40% mass reduction ball should experience bending stresses due to centrifugal loading that are 68% of those experienced by a 50% mass reduction ball.

REFERENCES

1. Anderson, W.J., Fleming, D.L., and Parker, R.J., "The Series Hybrid Bearing - A New High Speed Bearing Concept", Journal of Lubrication Technology, Trans. ASME, Series F, Vol. 94, No. 2, April, 1972, pp 117 - 124.

2. Coe, H.H., Parker, R.J., and Scibbe, H.W., "Evaluation of Electron-Beam Welded Hollow Balls for High-Speed Ball Bearings", Journal of Lubrication Technology, Trans. ASME, Series F., Vol. 93, No. 1, Jan., 1971, pp. 47 - 59.

3. Dally, J.W., and Riley, W.F., Experimental Stress Analysis, McGraw-Hill Book Company, New York, 1965.

4. Golecki, J., The Sphere Weakened by a Concentric Inclusion of Different Elastic Properties Under Concentrated Loads, Archiwum Mechaniki Stosowanej, Vol. 9, 1957, pp 301 - 317.

5. Pih, H., and Vanderveldt, H., Stresses in Spheres with Concentric Spherical Cavities Under Diametral Compression by Three-Dimensional Photoelasticity, Experimental Mechanics, May 1966, pp. 244 - 250.

6. Rumbarger, J.H., Herrick, R.C., and Eklund, P.R., Analysis of the Elastic Contact of a Hollow Ball with a Flat Plate, Journal of Lubrciation Technology, Trans. A.S.M.E., Series F., Vol. 92, No. 1, Jan., 1970, pp. 138 - 144.

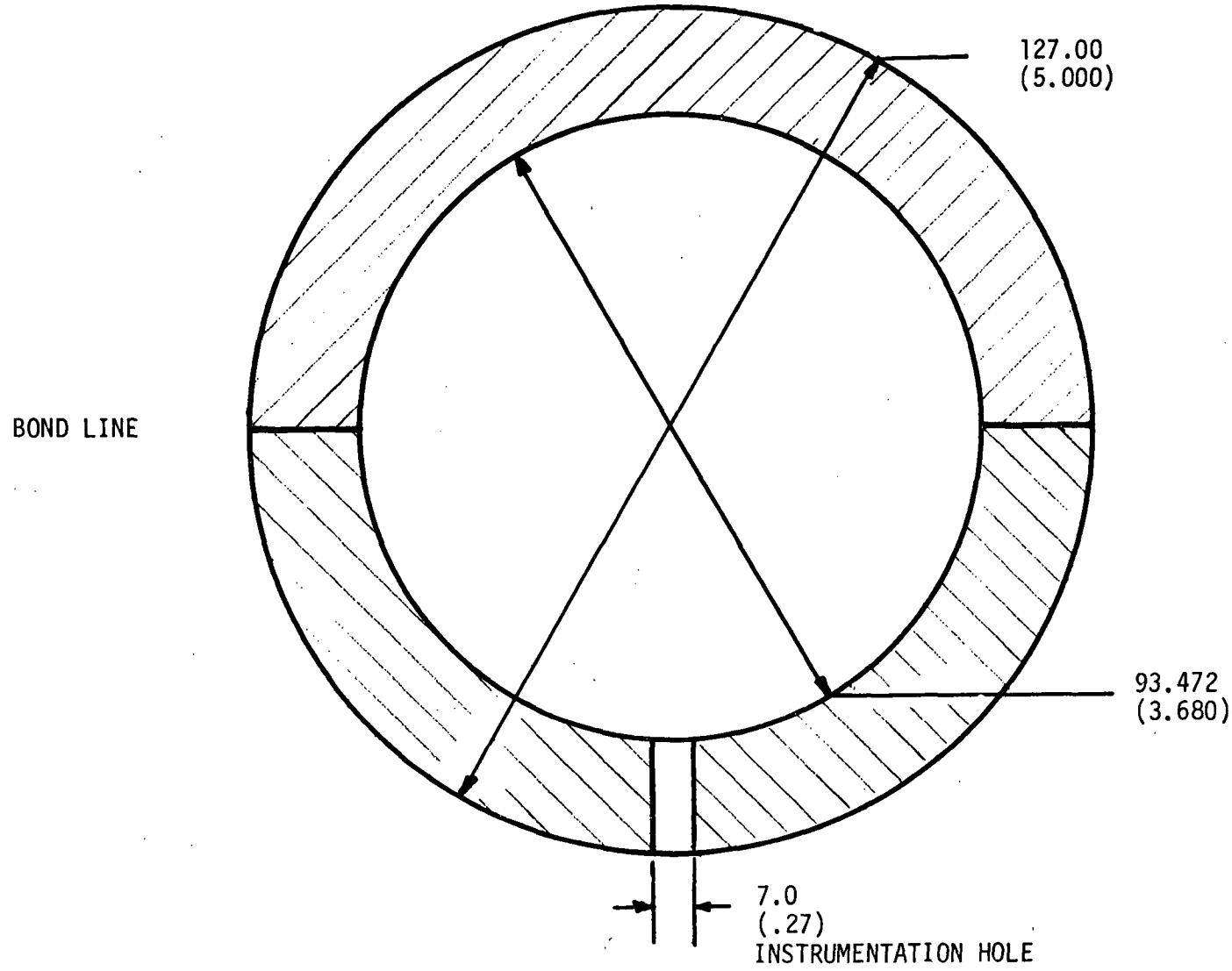

FIG. 1a FORTY % MASS REDUCTION MODEL DIMENSIONS MM (IN)

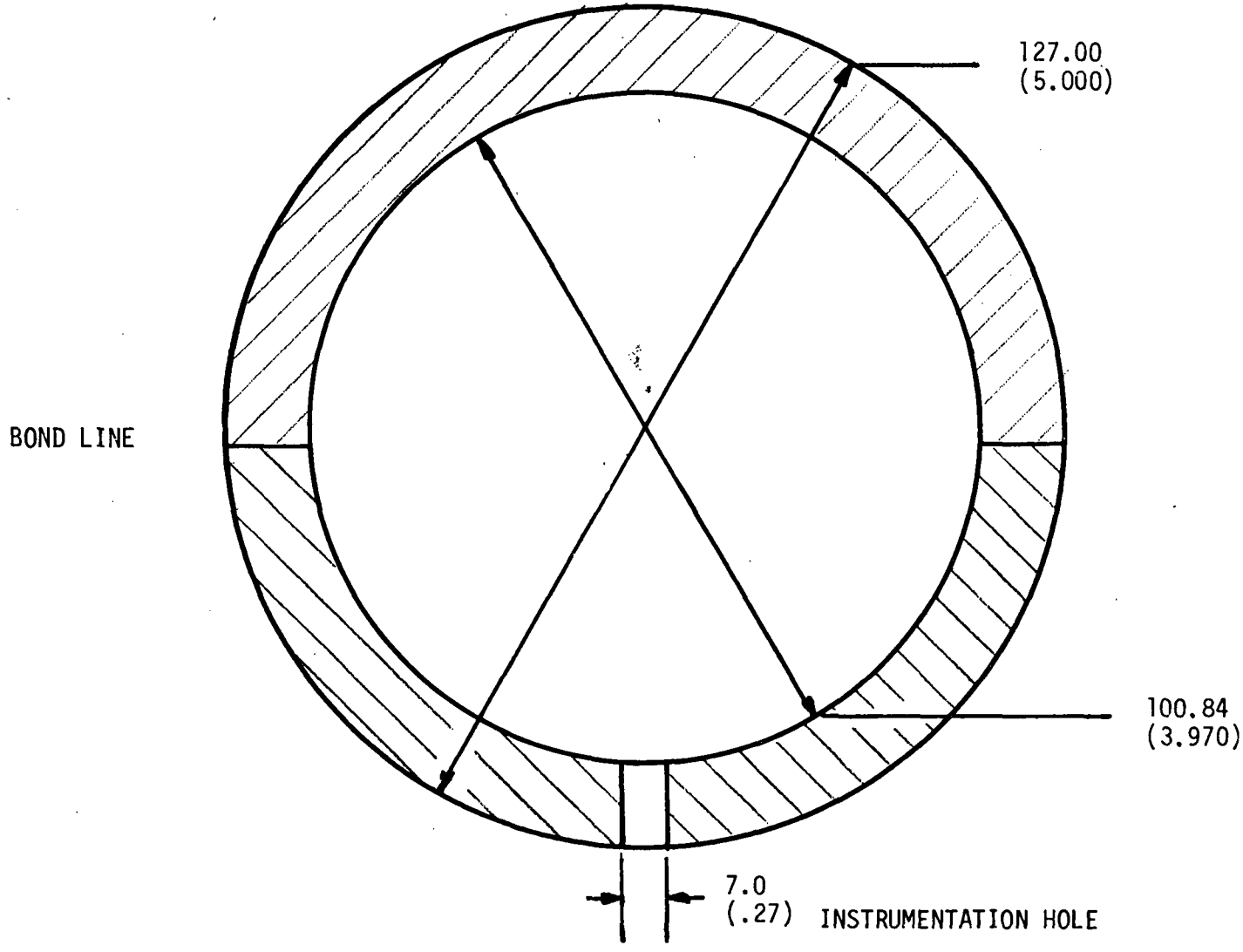

FIG. 1b FIFTY % MASS REDUCTION MODEL DIMENSIONS MM (IN)

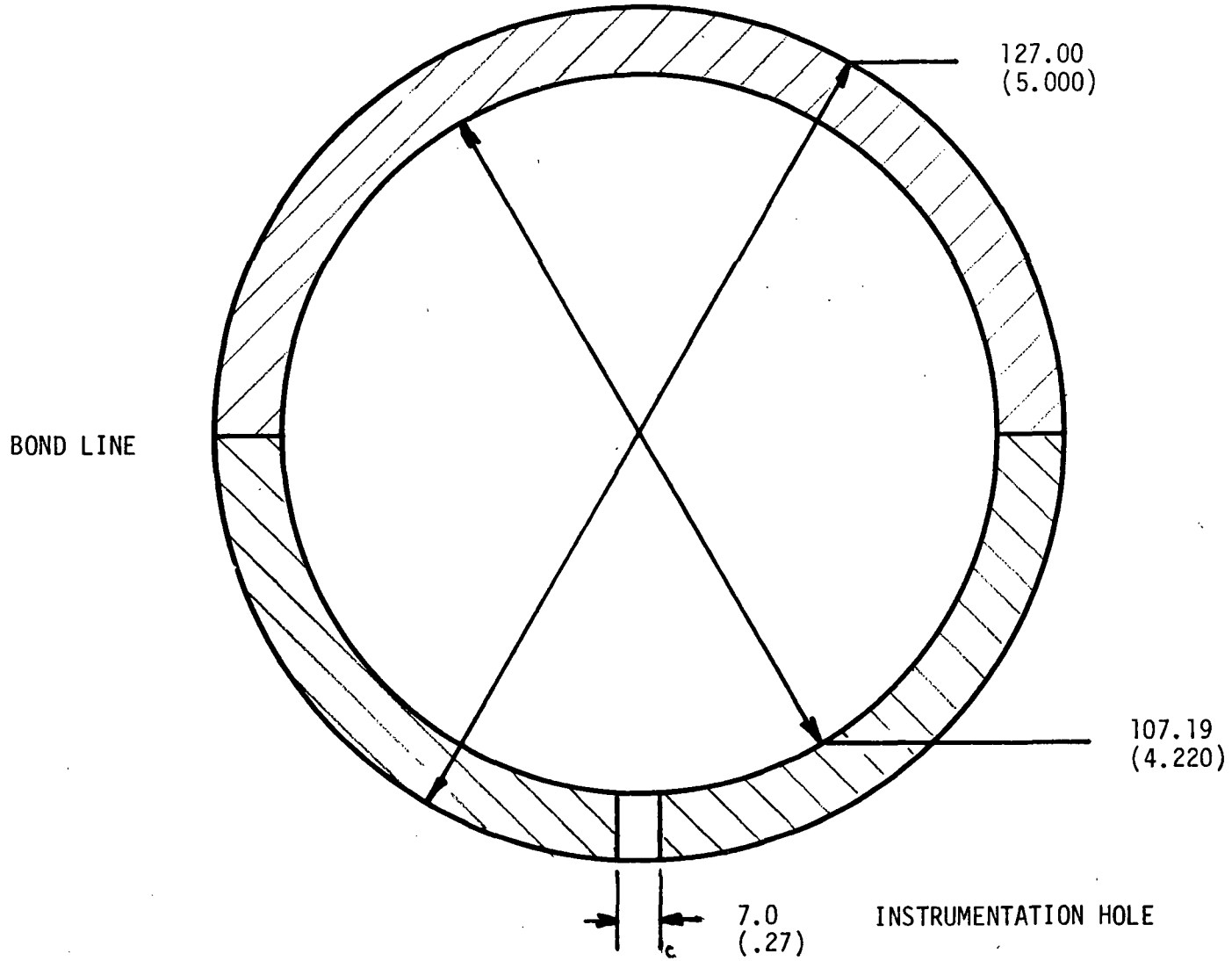

FIG. 1c SIXTY % MASS REDUCTION MODEL DIMENSIONS MM (IN)

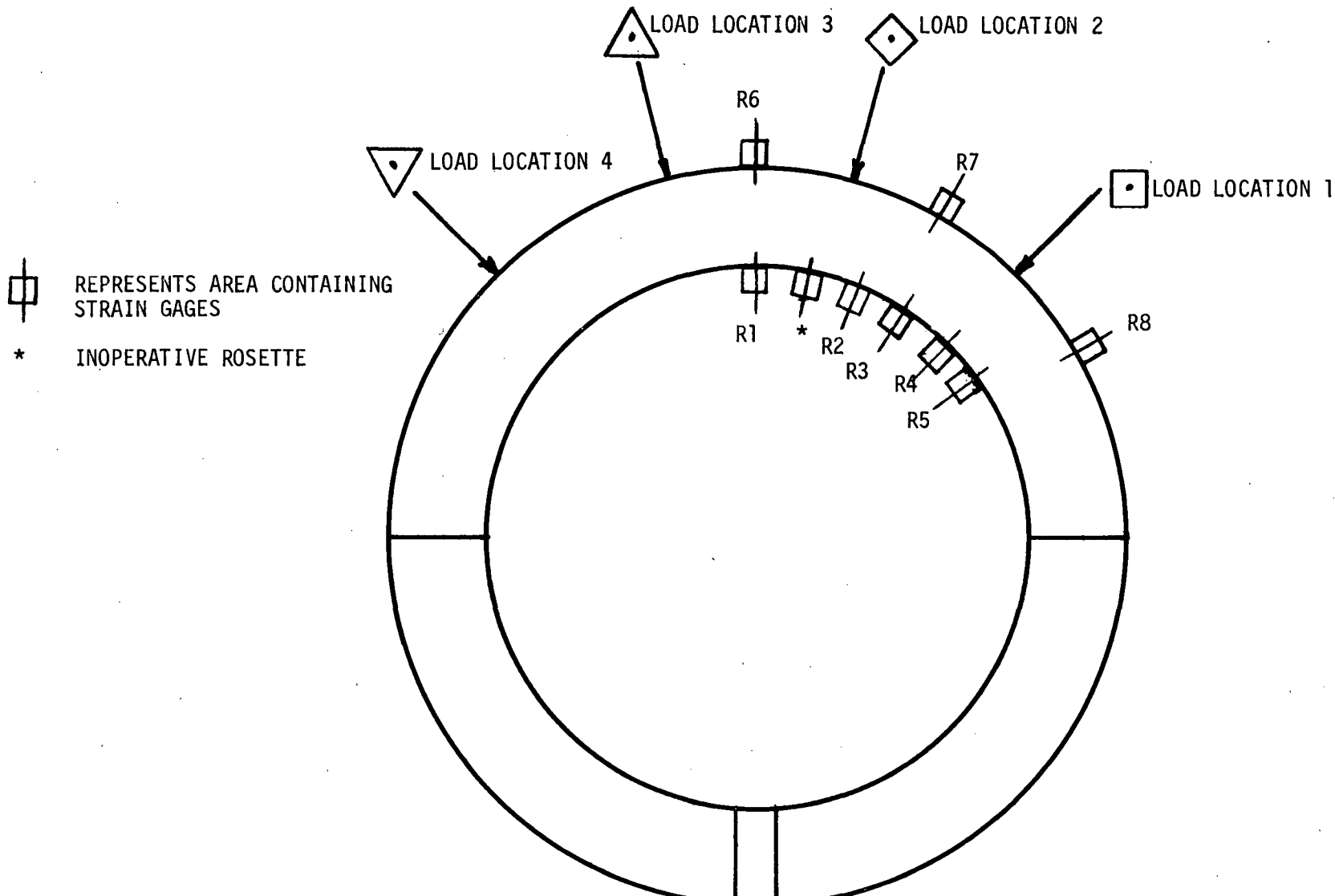

FIG. 2a ROSETTE AND LOAD LOCATIONS ON 40% MASS REDUCTION MODEL

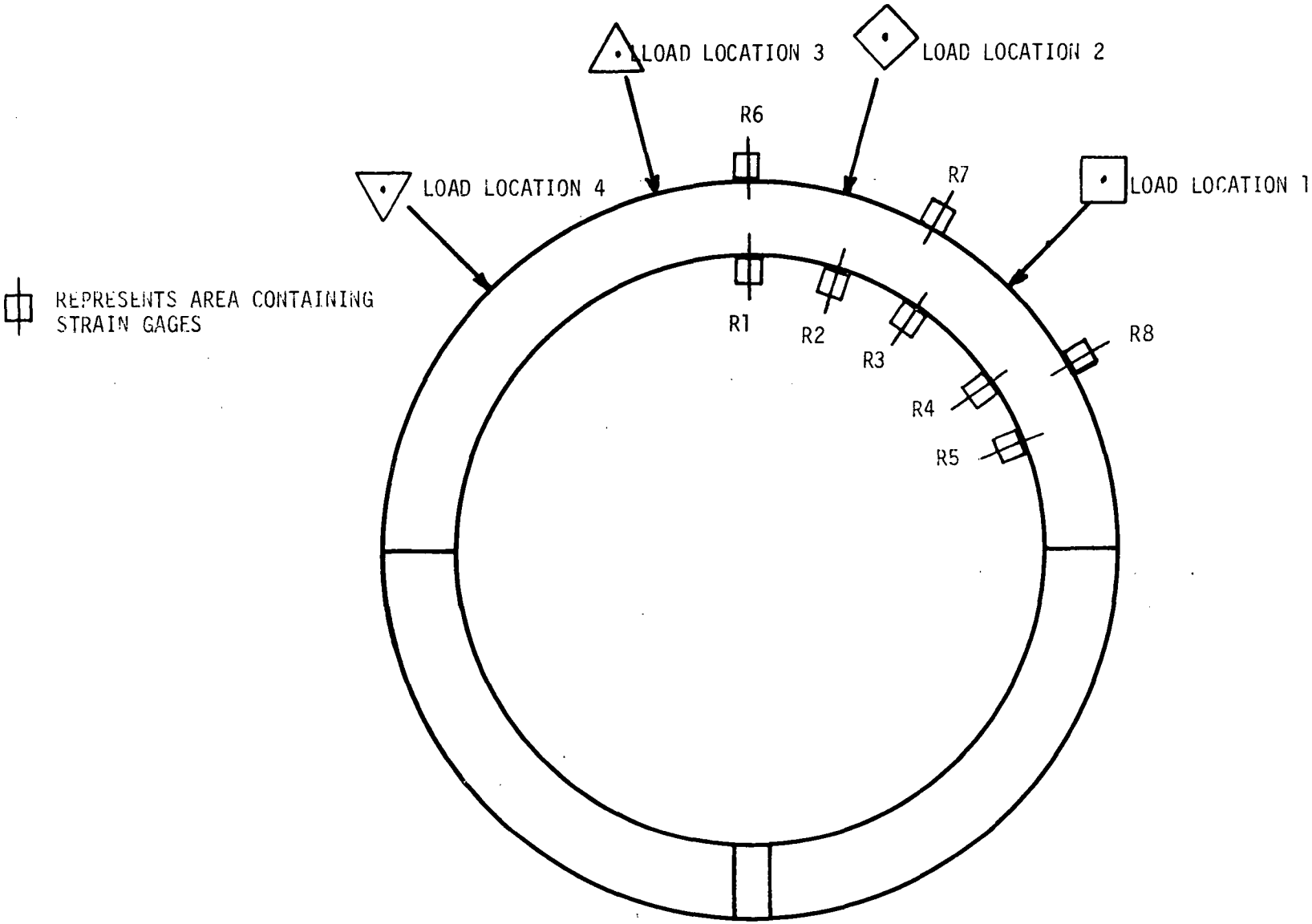

FIG. 2b ROSETTE AND LOAD LOCATIONS
ON 50% MASS REDUCTION MODEL

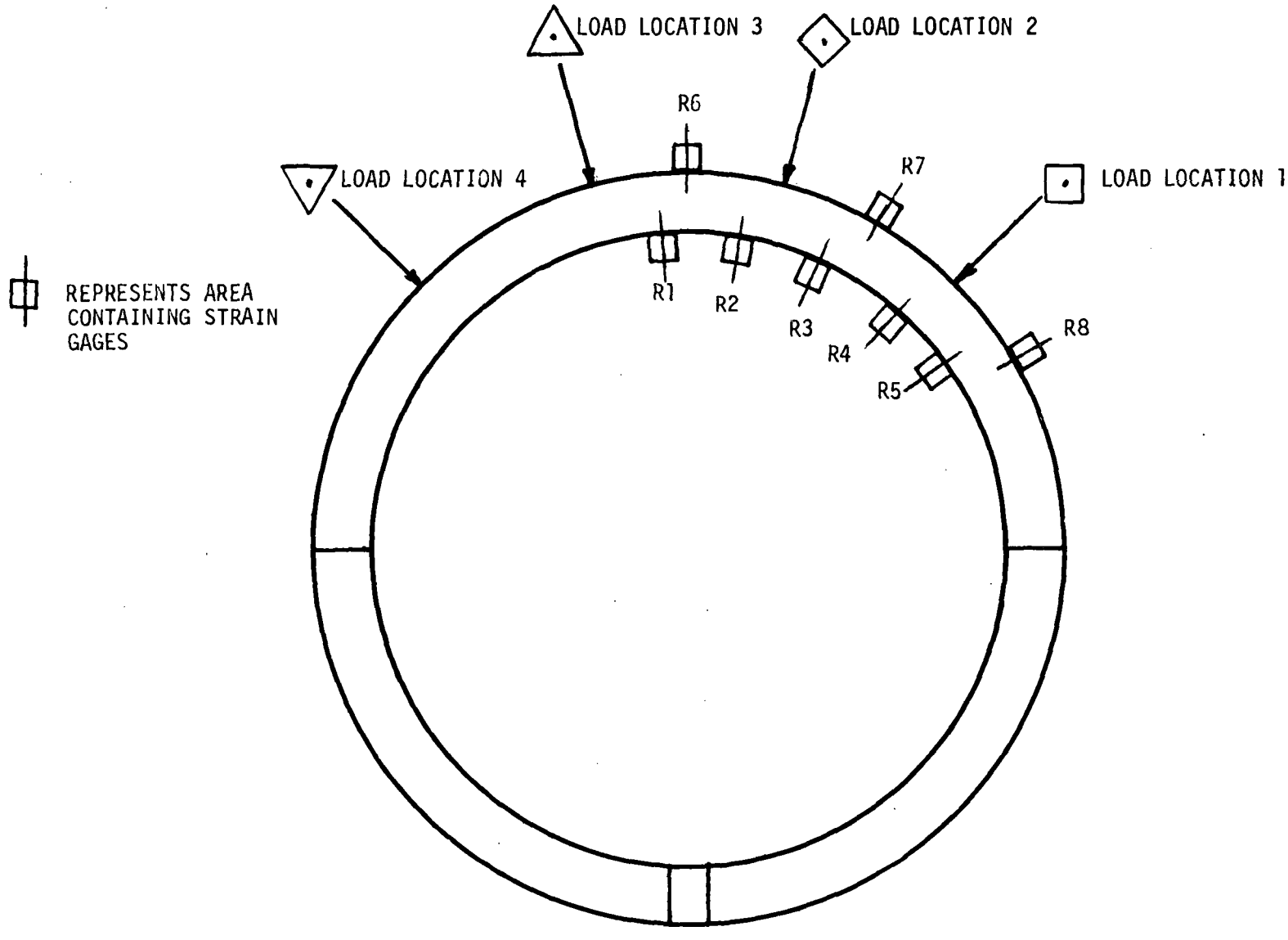

FIG. 2c ROSETTE AND LOAD LOCATIONS ON 60% MASS REDUCTION MODEL

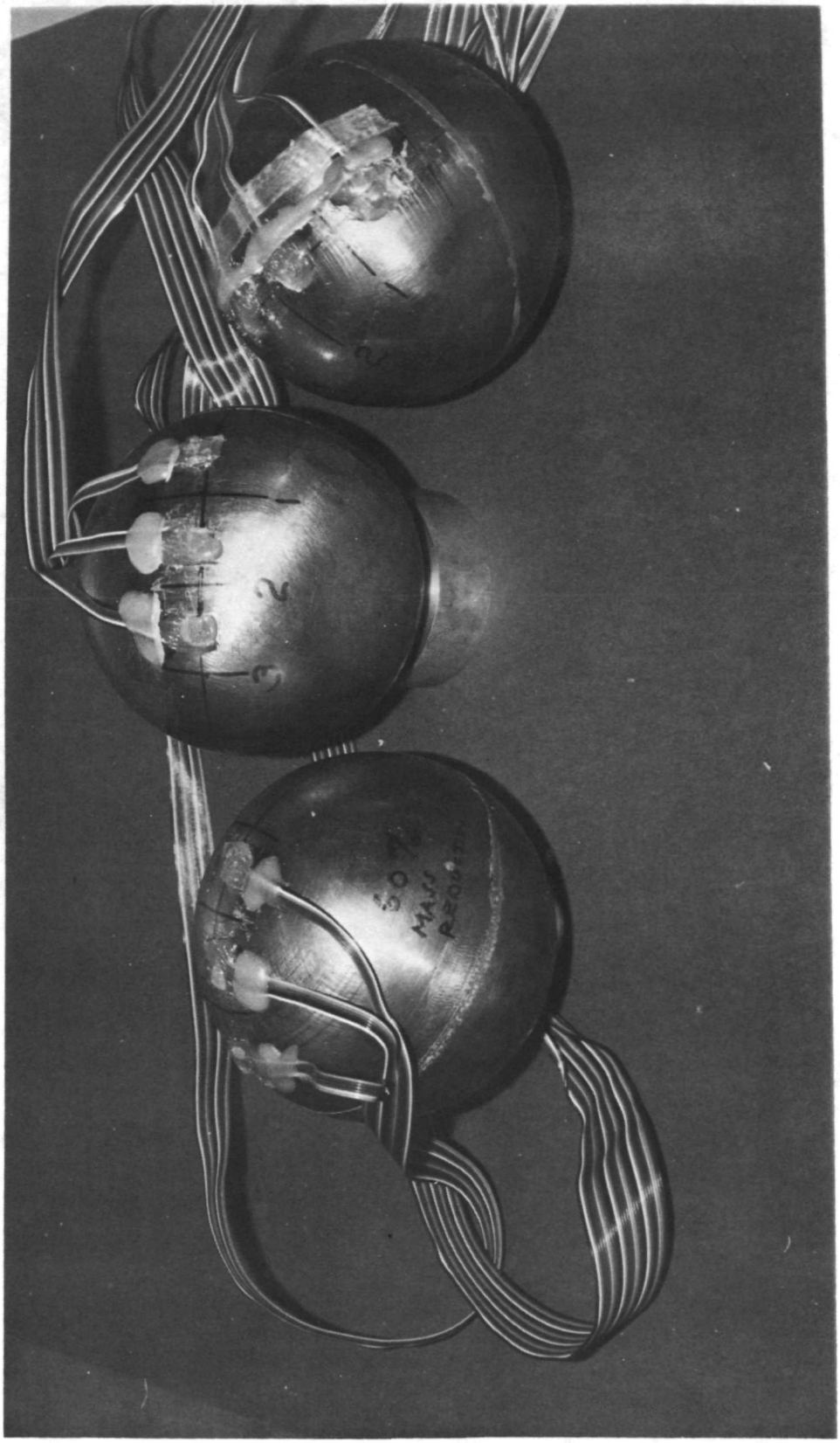

FIGURE 3 MODELS USED

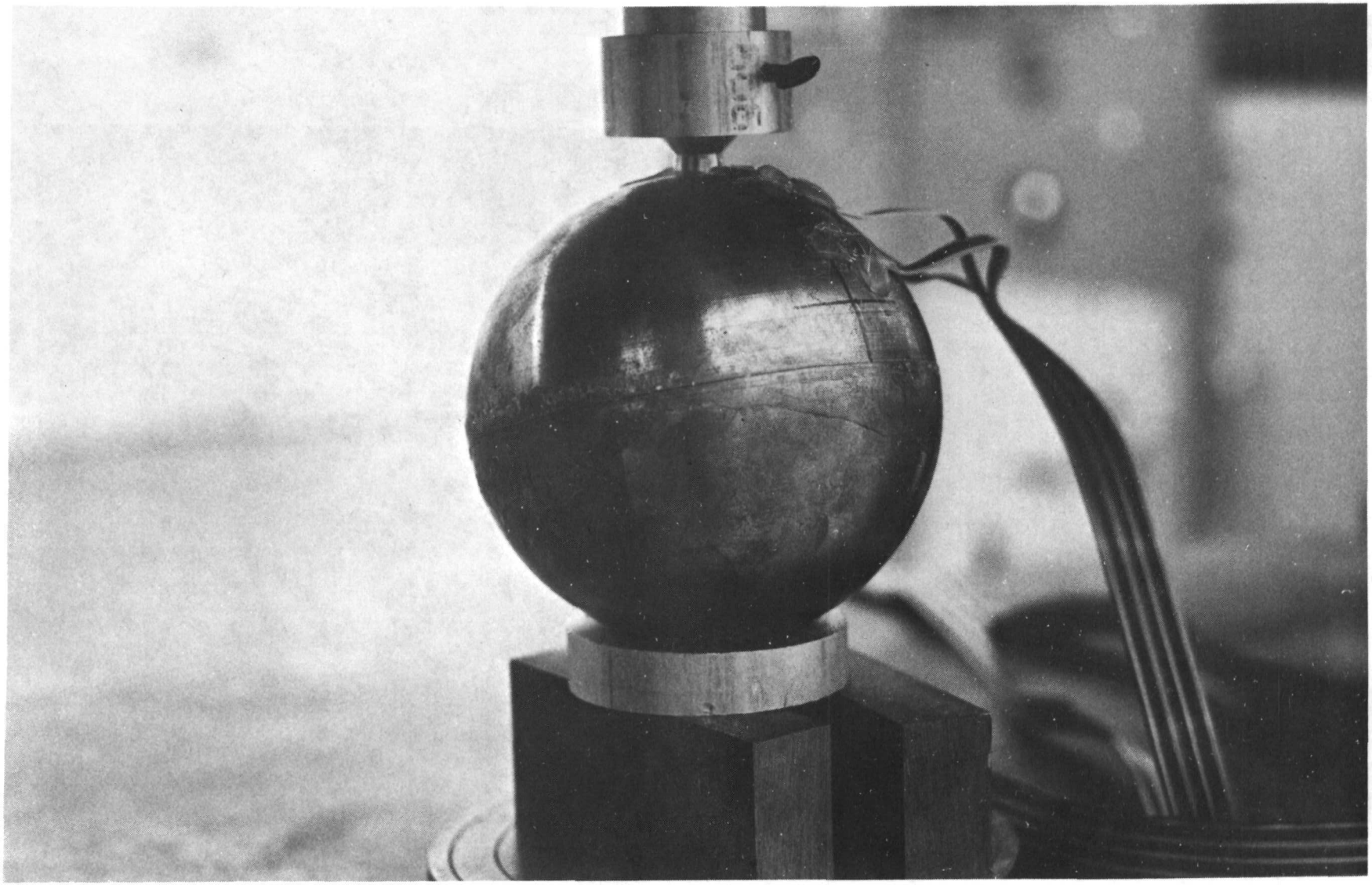

FIG. 4 PHOTOGRAPH OF MODEL
POSITIONED FOR TESTING

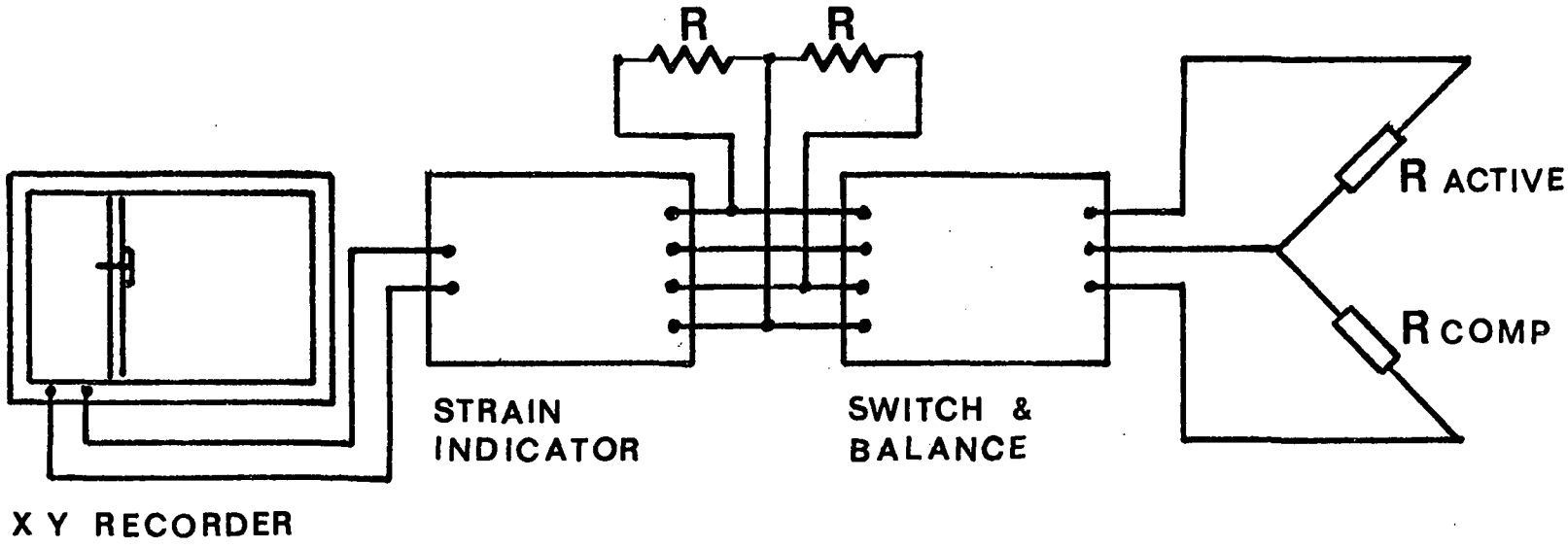

FIG 5 CIRCUIT DIAGRAM OF INSTRUMENTATION

FIG. 6 PHOTOGRAPH OF
APPARATUS USED

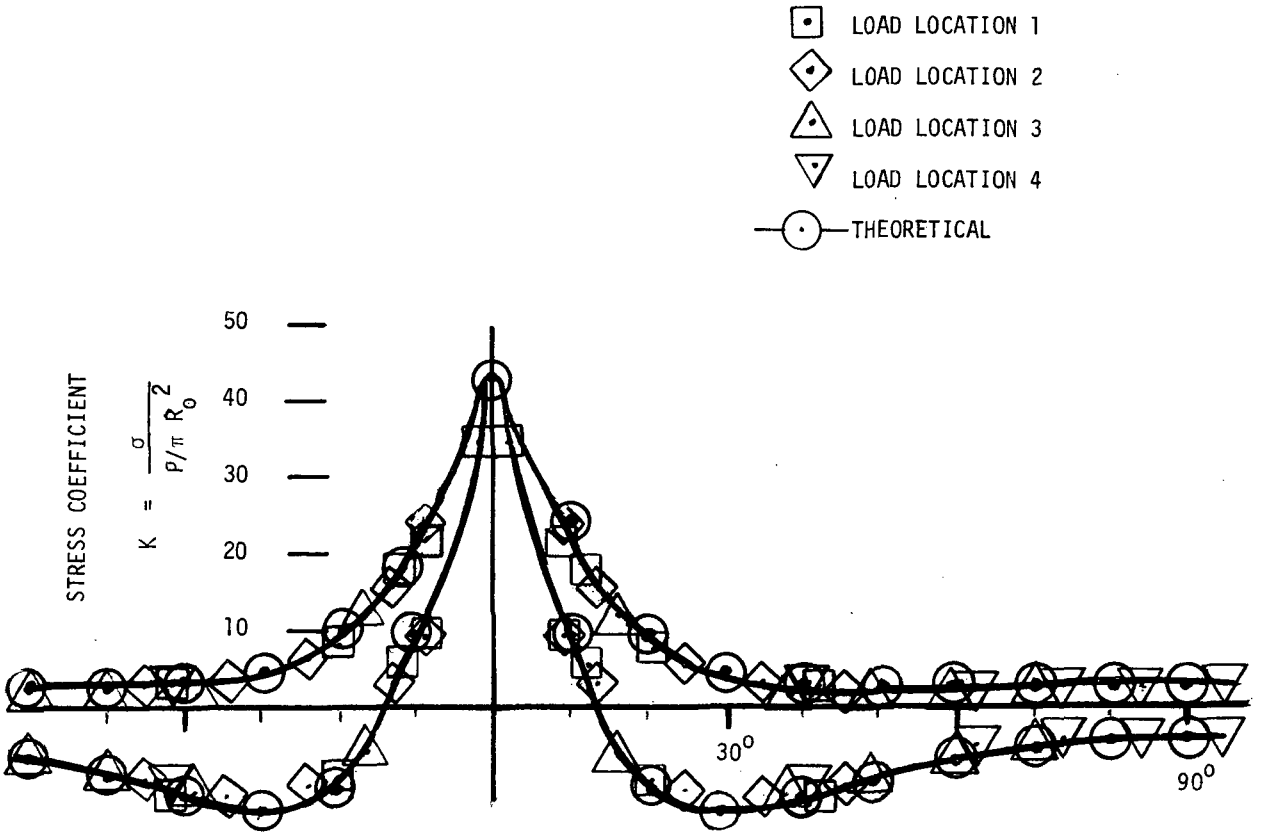

FIG. 7a DIMENSIONLESS PRINCIPAL STRESS COEFFICIENTS FOR 40% MASS REDUCTION MODEL INTERIOR LOAD LOCATIONS SHOWN IN FIGURE 2a.

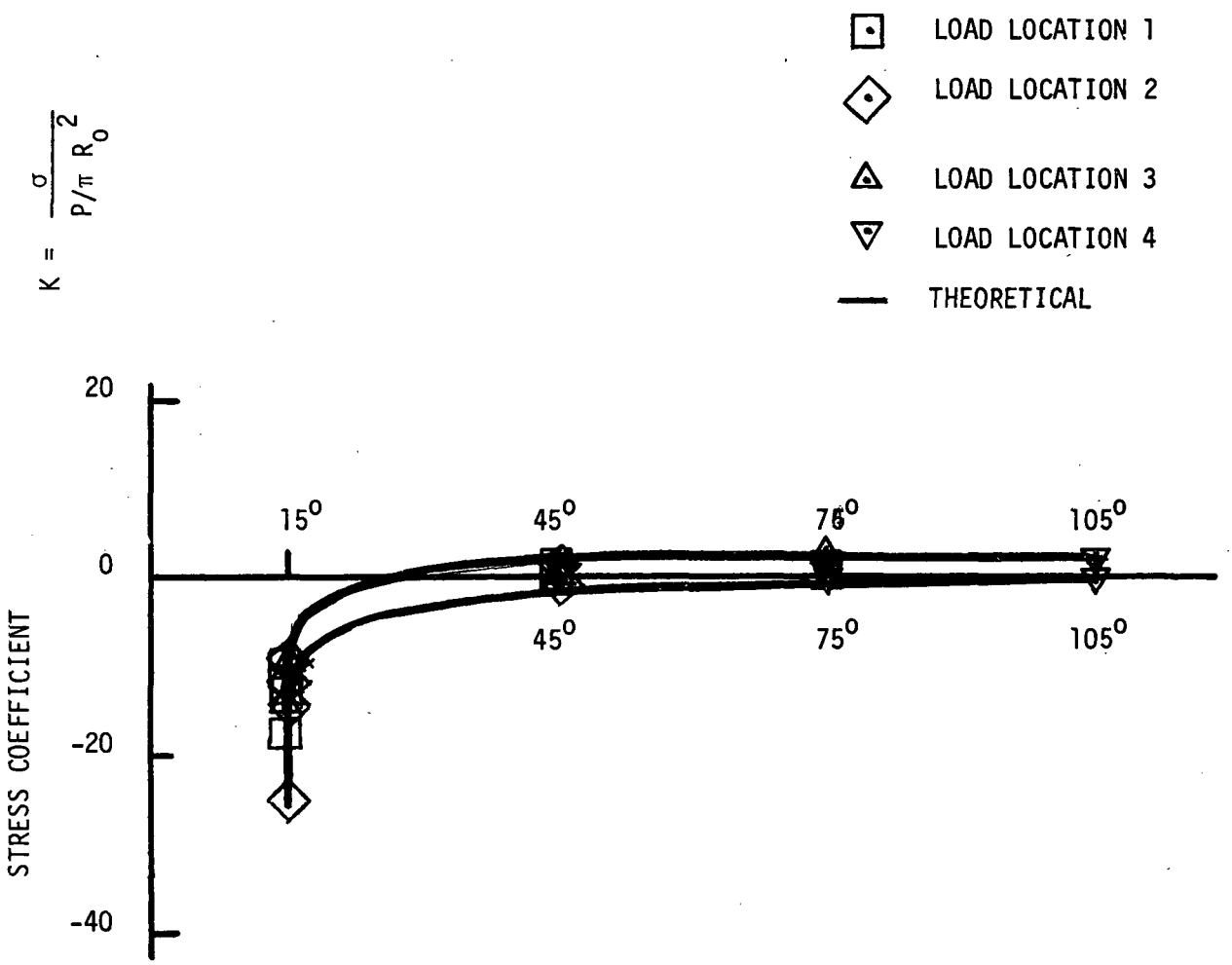

FIG. 7b DIMENSIONLESS PRINCIPAL STRESS COEFFICIENTS FOR 40% MASS REDUCTION MODEL EXTERIOR LOAD LOCATION SHOWN IN FIGURE 2a.

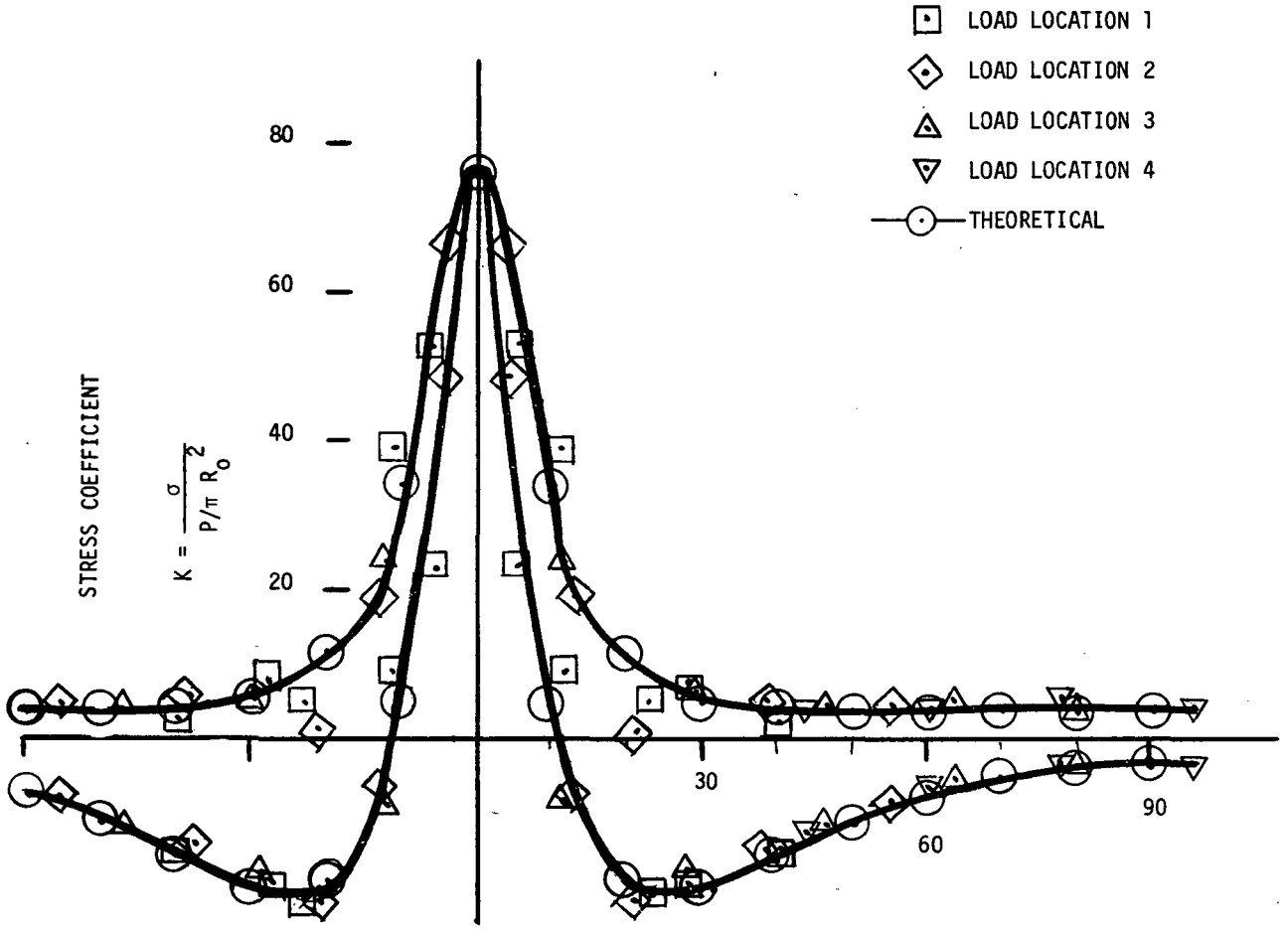

FIG. 8a DIMENSIONLESS PRINCIPAL STRESS COEFFICIENTS FOR 50% MASS REDUCTION MODEL INTERIOR LOAD LOCATION SHOWN IN FIGURE 2b.

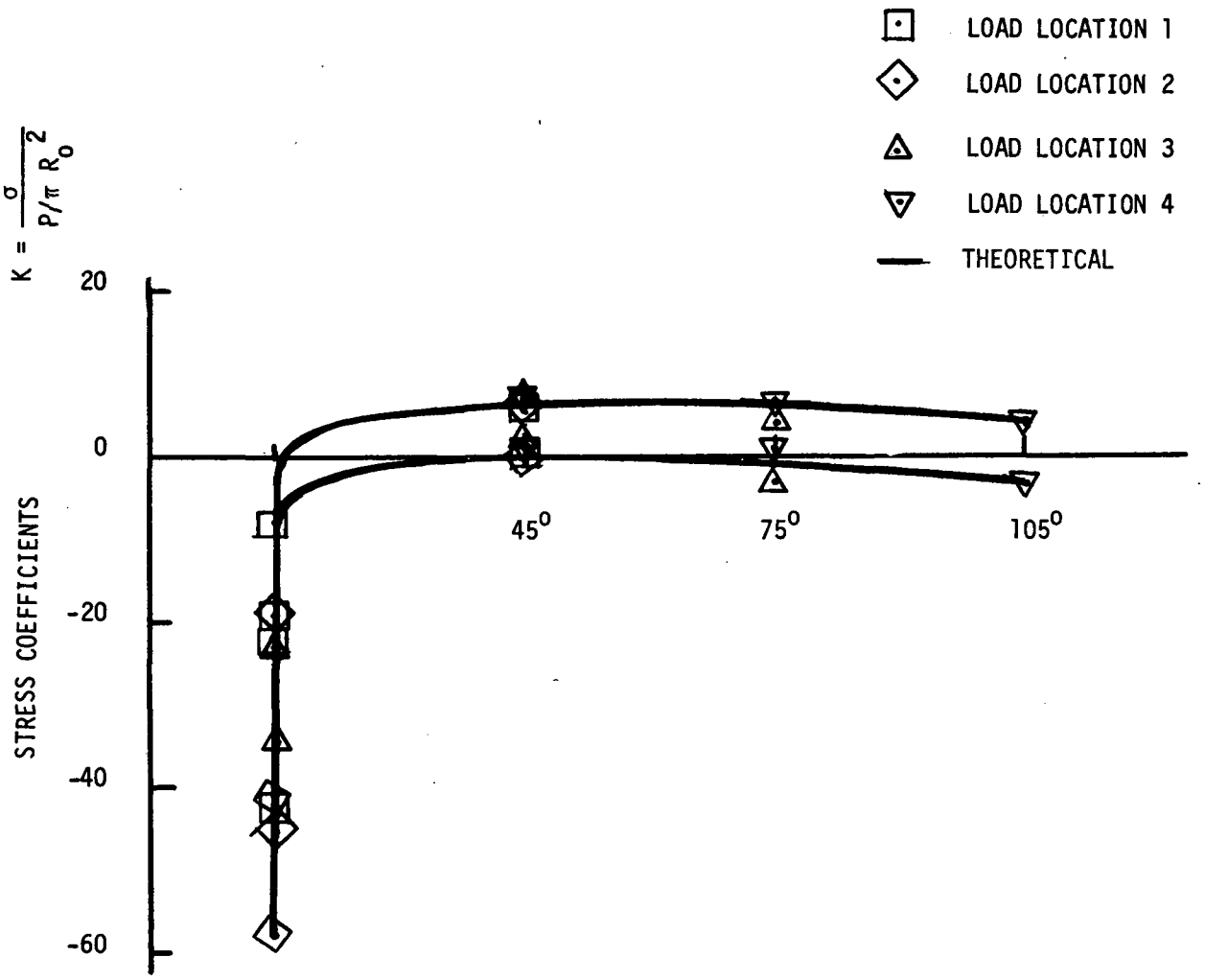

FIG. 9b DIMENSIONLESS PRINCIPAL STRESS COEFFICIENTS FOR 60% MASS REDUCTION MODEL EXTERIOR LOAD LOCATIONS SHOWN IN FIGURE 2(c).

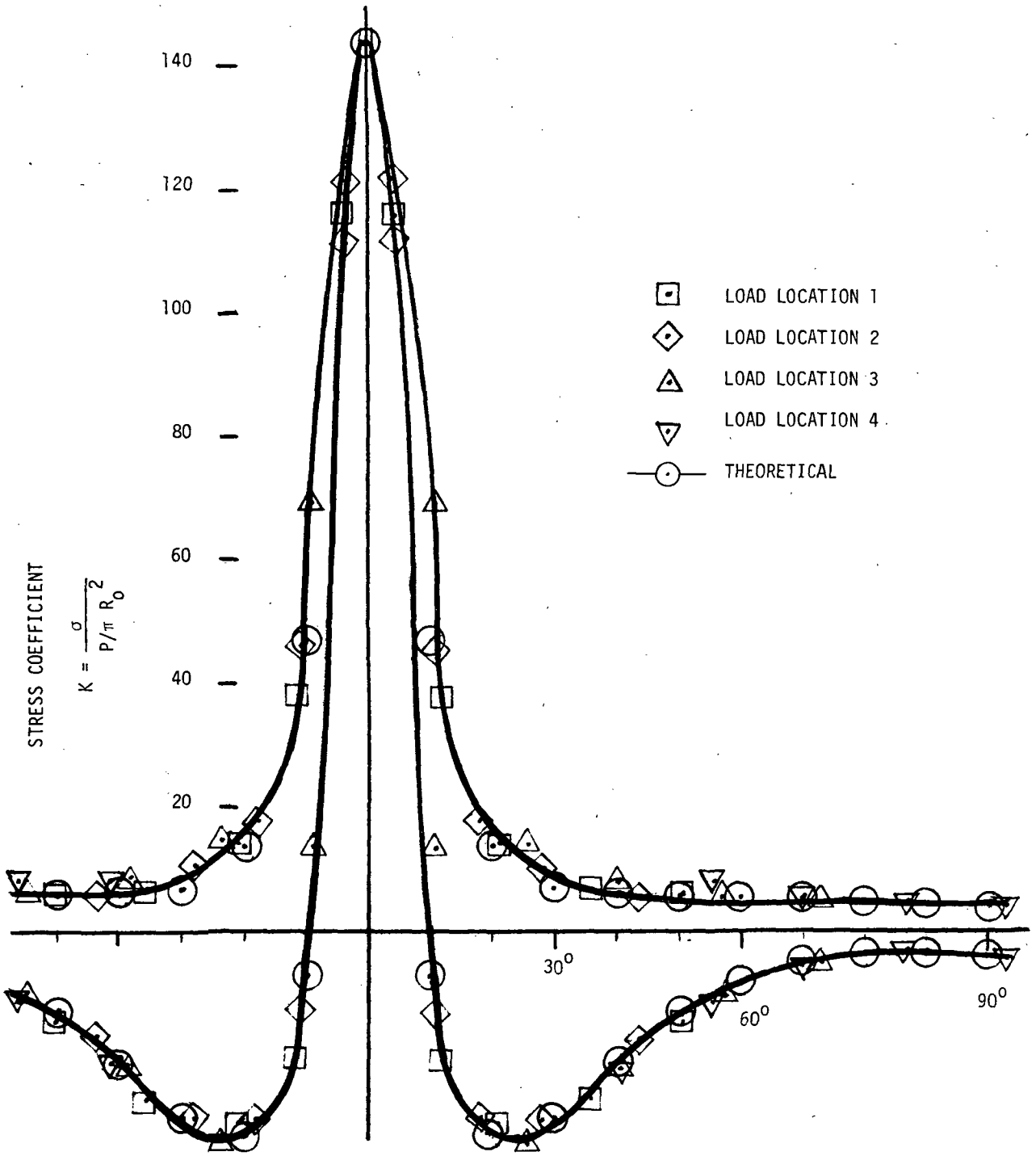

FIG. 9a DIMENSIONLESS PRINCIPAL STRESS COEFFICIENTS FOR 60% MASS REDUCTION MODEL INTERIOR LOAD LOCATIONS SHOWN IN FIGURE 2c

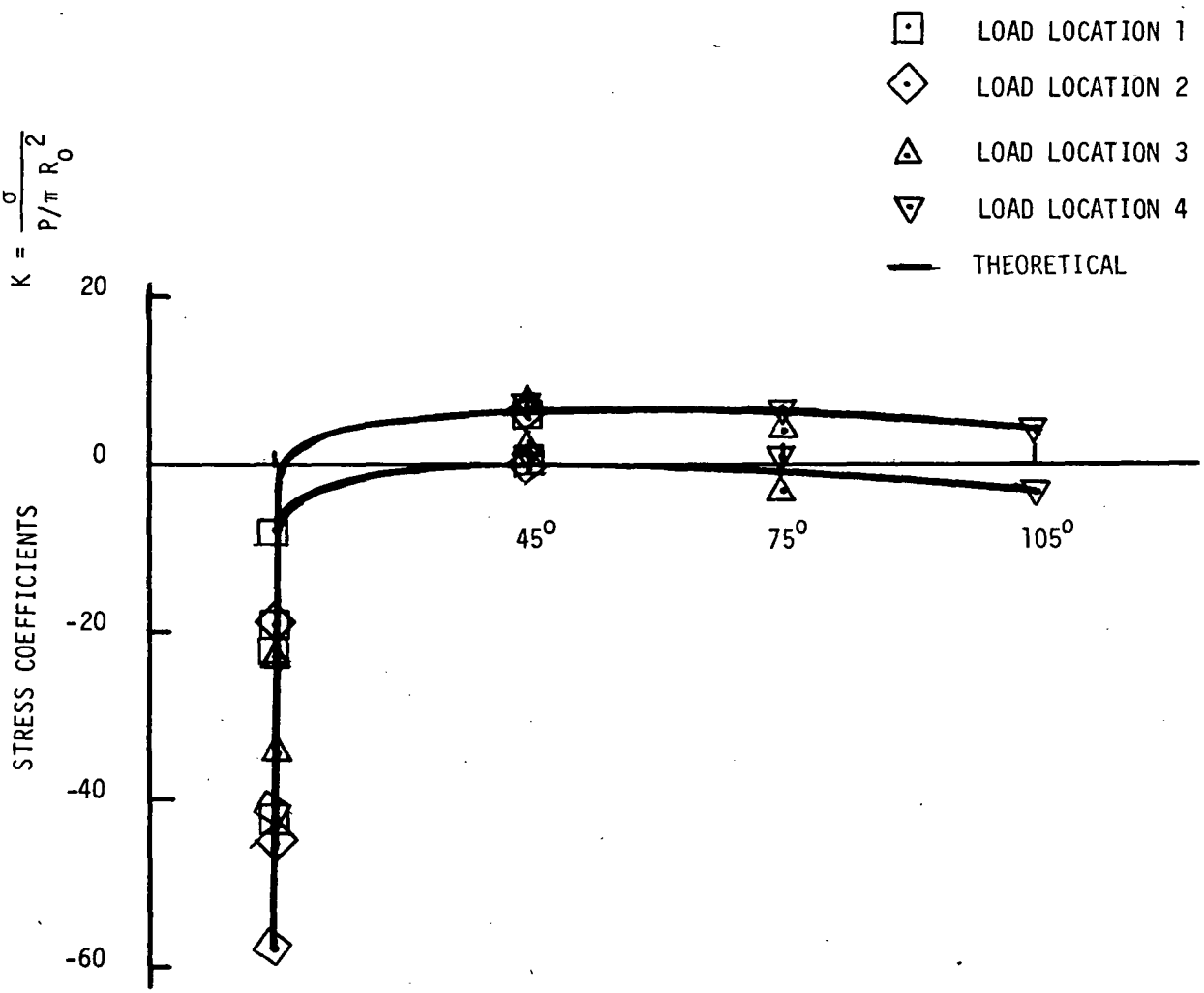

FIG. 9b DIMENSIONLESS PRINCIPAL STRESS COEFFICIENTS FOR 60% MASS REDUCTION MODEL EXTERIOR LOAD LOCATIONS SHOWN IN FIGURE 2(c).

TABLE I

ROSETTE ANGULAR LOCATION ON GREAT CIRCLE
FROM CENTER OF HEMISPHERE

40% MASS REDUCTION MODEL

Interior		Exterior	
Rosette Number	Angle Degrees	Rosette Number	Angle Degrees
1	0	1	0^{o}
2	22.0*	2	30
3	33.4	3	60
4	43.3		
5	54.2		

50% MASS REDUCTION MODEL

Interior		Exterior	
Rosette Number	Angle Degrees	Rosette Number	Angle Degrees
1	0	1	0^{o}
2	17.2	2	30
3	34.4	3	60
4	51.7		
5	68.4		

60% MASS REDUCTION MODEL

Interior		Exterior	
Rosette Number	Angle Degrees	Rosette Number	Angle Degrees
1	-4.9	1	0^{o}
2	9.2	2	30
3	24.2	3	60
4	41.3		
5	54.1		

* Six rosettes were mounted in the 40% mass reduction model, however, a rosette at 11^{o} was found to be inoperative.

TABLE 2a

DATA, PRINCIPAL STRAINS, AND DIMENSIONLESS PRINCIPAL STRESS COEFFICIENTS FOR A 17,800 N (4,000 LB) LOAD AT LOAD LOCATION 1 ON THE 40 PERCENT MASS REDUCTION MODEL

INTERIOR

ROSETTE NUMBER	EPSILON A MICRO M/M	EPSILON B MICRO M/M	EPSILON C MICRO M/M	EPSILON 1 MICRO M/M	EPSILON 2 MICRO M/M	SIGMA 1*RO*RO*PI/P DIMENSIONLESS	SIGMA 2*RO*RO*PI/P DIMENSIONLESS
1	-80.00	-12.40	42.20	42.54	-80.34	2.984	-10.936
2	-77.60	16.00	74.60	76.59	-79.59	8.530	-9.161
3	24.40	93.00	127.80	130.49	21.71	22.171	9.848
4	168.00	166.20	164.40	168.00	164.40	35.168	34.760
5	13.80	27.40	102.20	111.76	4.24	18.291	6.112

EXTERIOR

ROSETTE NUMBER	EPSILON A MICRO M/M	EPSILON B MICRO M/M	EPSILON C MICRO M/M	EPSILON 1 MICRO M/M	EPSILON 2 MICRO M/M	SIGMA 1*RO*RO*PI/P DIMENSIONLESS	SIGMA 2*RO*RO*PI/P DIMENSIONLESS
1	-2.80	2.80	6.00	6.16	-2.96	0.853	-0.180
2	-40.40	-53.00	-92.40	-97.15	-95.65	-10.655	-17.282
3	-38.80	-54.20	-61.00	-38.00	-61.80	-9.149	-11.846

TABLE 2b

DATA, PRINCIPAL STRAINS, AND DIMENSIONLESS PRINCIPAL STRESS COEFFICIENTS FOR A 17,800 N (4,000 LB) LOAD AT LOAD LOCATION 2 ON THE 40 PERCENT MASS REDUCTION MODEL

INTERIOR

ROSETTE NUMBER	EPSILON A MICRO M/M	EPSILON B MICRO M/M	EPSILON C MICRO M/M	EPSILON 1 MICRO M/M	EPSILON 2 MICRO M/M	SIGMA 1*RO*RO*PI/P DIMENSIONLESS	SIGMA 2*RO*RO*PI/P DIMENSIONLESS
1	16.20	105.20	137.20	143.58	9.82	23.711	8.560
2	10.00	4.20	79.60	98.27	-8.67	15.482	3.367
3	-80.40	-31.00	58.60	61.45	-83.25	5.902	-10.489
4	-83.20	-18.40	46.40	46.40	-83.20	3.470	-11.211
5	-70.80	-24.80	37.20	37.79	-71.39	2.650	-9.718

EXTERIOR

ROSETTE NUMBER	EPSILON A MICRO M/M	EPSILON B MICRO M/M	EPSILON C MICRO M/M	EPSILON 1 MICRO M/M	EPSILON 2 MICRO M/M	SIGMA 1*RO*RO*PI/P DIMENSIONLESS	SIGMA 2*RO*RO*PI/P DIMENSIONLESS
1	-45.20	-70.00	-134.40	-41.00	-138.60	-13.364	-24.419
2	-35.40	-50.40	-57.40	-34.70	-58.10	-8.435	-11.087
3	-4.00	3.20	15.00	15.27	-4.27	2.264	0.050

TABLE 2c

DATA, PRINCIPAL STRAINS, AND DIMENSIONLESS PRINCIPAL STRESS COEFFICIENTS FOR A 17,800 N (4,000 LB) LOAD AT LOAD LOCATION 3 ON THE 40 PERCENT MASS REDUCTION MODEL

INTERIOR

ROSETTE NUMBER	EPSILON A MICRO M/M	EPSILON B MICRO M/M	EPSILON C MICRO M/M	EPSILON 1 MICRO M/M	EPSILON 2 MICRO M/M	SIGMA 1*RO*RO*PI/P DIMENSIONLESS	SIGMA 2*RO*RO*PI/P DIMENSIONLESS
1	-40.80	-42.80	68.60	92.68	-64.88	11.849	-6.000
2	-75.80	-35.20	33.60	35.39	-77.59	1.960	-10.838
3	-66.80	-23.80	34.20	34.75	-67.35	2.354	-9.212
4	-49.80	-9.40	30.40	30.40	-49.80	2.502	-6.583
5	-38.60	-10.40	27.40	27.75	-38.95	2.599	-4.956

EXTERIOR

ROSETTE NUMBER	EPSILON A MICRO M/M	EPSILON B MICRO M/M	EPSILON C MICRO M/M	EPSILON 1 MICRO M/M	EPSILON 2 MICRO M/M	SIGMA 1*RO*RO*PI/P DIMENSIONLESS	SIGMA 2*RO*RO*PI/P DIMENSIONLESS
1	-40.60	-59.80	-64.80	-38.67	-66.73	-9.498	-12.676
2	-3.40	4.00	10.80	10.81	-3.41	1.583	-0.027
3	-9.60	3.80	19.80	19.86	-9.66	2.745	-0.599

TABLE 2d

DATA, PRINCIPAL STRAINS, AND DIMENSIONLESS PRINCIPAL STRESS COEFFICIENTS FOR A 17,800 N (4,000 LB) LOAD AT LOAD LOCATION 4 ON THE 40 PERCENT MASS REDUCTION MODEL

INTERIOR

ROSETTE NUMBER	EPSILON A MICRO M/M	EPSILON B MICRO M/M	EPSILON C MICRO M/M	EPSILON 1 MICRO M/M	EPSILON 2 MICRO M/M	SIGMA 1*RO*RO*PI/P DIMENSIONLESS	SIGMA 2*RO*RO*PI/P DIMENSIONLESS
1	-68.20	-31.40	34.80	36.86	-70.26	2.554	-9.580
2	-37.20	-9.80	24.80	25.01	-37.41	2.231	-4.840
3	-33.00	-6.60	25.80	25.95	-33.15	2.590	-4.105
4	-29.00	-0.80	27.40	27.40	-29.00	3.026	-3.363
5	-32.00	-6.80	27.60	27.95	-32.35	2.953	-3.879

EXTERIOR

ROSETTE NUMBER	EPSILON A MICRO M/M	EPSILON B MICRO M/M	EPSILON C MICRO M/M	EPSILON 1 MICRO M/M	EPSILON 2 MICRO M/M	SIGMA 1*RO*RO*PI/P DIMENSIONLESS	SIGMA 2*RO*RO*PI/P DIMENSIONLESS
1	-2.60	5.20	13.20	13.20	-2.60	2.010	0.220
2	-10.60	5.60	19.60	19.64	-10.64	2.662	-0.768
3	-9.80	3.40	19.60	19.68	-9.88	2.705	-0.643

TABLE 3a

DATA, PRINCIPAL STRAINS, AND DIMENSIONLESS PRINCIPAL STRESS COEFFICIENTS FOR A 11,120 N (2,500 LB) LOAD AT LOAD LOCATION 1 ON THE 50 PERCENT MASS REDUCTION MODEL

INTERIOR

ROSETTE NUMBER	EPSILON A MICRO M/M	EPSILON B MICRO M/M	EPSILON C MICRO M/M	EPSILON 1 MICRO M/M	EPSILON 2 MICRO M/M	SIGMA 1*RO*RO*PI/P DIMENSIONLESS	SIGMA 2*RO*RO*PI/P DIMENSIONLESS
1	31.60	-13.00	-67.00	31.82	-67.22	3.018	-14.934
2	47.20	-2.40	-92.20	50.04	-95.04	5.574	-20.721
3	194.60	112.80	31.00	194.60	31.00	52.794	23.142
4	143.40	31.20	-0.60	153.86	-11.06	38.979	9.087
5	58.00	-16.40	-91.40	58.00	-91.40	7.918	-19.160

EXTERIOR

ROSETTE NUMBER	EPSILON A MICRO M/M	EPSILON B MICRO M/M	EPSILON C MICRO M/M	EPSILON 1 MICRO M/M	EPSILON 2 MICRO M/M	SIGMA 1*RO*RO*PI/P DIMENSIONLESS	SIGMA 2*RO*RO*PI/P DIMENSIONLESS
1	-2.00	5.60	9.60	9.87	-2.27	2.380	0.178
2	-28.60	-41.60	-91.20	-23.64	-96.16	-13.591	-26.734
3	-21.80	-40.40	-42.60	-18.96	-45.44	-8.438	-13.239

TABLE 3b

DATA, PRINCIPAL STRAINS, AND DIMENSIONLESS PRINCIPAL STRESS COEFFICIENTS FOR A 11,120 N (2,500 LB) LOAD AT LOAD LOCATION 2 ON THE 50 PERCENT MASS REDUCTION MODEL

INTERIOR

ROSETTE NUMBER	EPSILON A MICRO M/M	EPSILON B MICRO M/M	EPSILON C MICRO M/M	EPSILON 1 MICRO M/M	EPSILON 2 MICRO M/M	SIGMA 1*RO*RO*PI/P DIMENSIONLESS	SIGMA 2*RO*RO*PI/P DIMENSIONLESS
1	88.00	36.40	-50.00	90.16	-52.16	19.293	-6.502
2	211.40	144.00	130.80	219.66	122.54	66.394	48.790
3	33.00	-29.80	-92.80	33.00	-92.80	1.336	-21.465
4	42.80	-20.20	-70.20	43.17	-70.57	5.697	-14.919
5	31.40	-4.40	-40.20	31.40	-40.20	5.008	-7.970

EXTERIOR

ROSETTE NUMBER	EPSILON A MICRO M/M	EPSILON B MICRO M/M	EPSILON C MICRO M/M	EPSILON 1 MICRO M/M	EPSILON 2 MICRO M/M	SIGMA 1*RO*RO*PI/P DIMENSIONLESS	SIGMA 2*RO*RO*PI/P DIMENSIONLESS
1	-46.80	-63.60	-124.00	-41.07	-129.73	-20.711	-36.780
2	-37.20	-63.20	-72.80	-35.40	-74.60	-14.961	-22.065
3	-3.60	7.40	17.20	17.22	-3.62	4.177	0.401

TABLE 3c

DATA, PRINCIPAL STRAINS, AND DIMENSIONLESS PRINCIPAL STRESS COEFFICIENTS FOR A 11,120 N (2,500 LB) LOAD AT LOAD LOCATION 3 ON THE 50 PERCENT MASS REDUCTION MODEL

INTERIOR

ROSETTE NUMBER	EPSILON A MICRO M/M	EPSILON B MICRO M/M	EPSILON C MICRO M/M	EPSILON 1 MICRO M/M	EPSILON 2 MICRO M/M	SIGMA 1*RO*RO*PI/P DIMENSIONLESS	SIGMA 2*RO*RO*PI/P DIMENSIONLESS
1	111.80	35.20	-64.40	112.55	-65.15	24.081	-8.126
2	47.60	-8.00	-82.00	48.25	-82.65	6.073	-17.652
3	32.60	-10.60	-53.80	32.60	-53.80	4.262	-11.398
4	27.40	-4.00	-28.80	27.59	-28.99	4.892	-5.364
5	21.60	-0.20	-21.60	21.60	-21.60	3.915	-3.915

EXTERIOR

ROSETTE NUMBER	EPSILON A MICRO M/M	EPSILON B MICRO M/M	EPSILON C MICRO M/M	EPSILON 1 MICRO M/M	EPSILON 2 MICRO M/M	SIGMA 1*RO*RO*PI/P DIMENSIONLESS	SIGMA 2*RO*RO*PI/P DIMENSIONLESS
1	-41.20	-62.00	-72.40	-40.36	-73.24	-16.138	-22.099
2	0.80	7.00	12.80	12.80	0.80	3.377	1.201
3	-11.00	3.20	17.80	17.80	-11.00	3.755	-1.466

TABLE 3d

DATA, PRINCIPAL STRAINS, AND DIMENSIONLESS PRINCIPAL STRESS COEFFICIENTS FOR A 11,120 N (2,500 LB) LOAD AT LOAD LOCATION 4 ON THE 50 PERCENT MASS REDUCTION MODEL

INTERIOR

ROSETTE NUMBER	EPSILON A MICRO M/M	EPSILON B MICRO M/M	EPSILON C MICRO M/M	EPSILON 1 MICRO M/M	EPSILON 2 MICRO M/M	SIGMA 1*RO*RO*PI/P DIMENSIONLESS	SIGMA 2*RO*RO*PI/P DIMENSIONLESS
1	32.40	-2.60	-58.80	33.62	-60.02	4.042	-12.928
2	25.00	1.40	-32.60	25.47	-33.07	4.025	-6.583
3	29.00	4.00	-21.00	29.00	-21.00	5.878	-3.185
4	22.00	4.60	-18.00	22.17	-18.17	4.329	-2.982
5	22.00	-3.80	-29.60	22.00	-29.60	3.397	-5.955

EXTERIOR

ROSETTE NUMBER	EPSILON A MICRO M/M	EPSILON B MICRO M/M	EPSILON C MICRO M/M	EPSILON 1 MICRO M/M	EPSILON 2 MICRO M/M	SIGMA 1*RO*RO*PI/P DIMENSIONLESS	SIGMA 2*RO*RO*PI/P DIMENSIONLESS
1	-3.00	5.40	16.40	16.49	-3.09	4.029	0.481
2	-11.60	1.20	18.60	18.77	-11.77	3.946	-1.590
3	-10.40	0.40	18.40	18.84	-10.84	4.037	-1.344

TABLE 4a

DATA, PRINCIPAL STRAINS, AND DIMENSIONLESS PRINCIPAL STRESS COEFFICIENTS FOR A 6,670 N (1,500 LB) LOAD AT LOAD LOCATION 1 ON THE 60 PERCENT MASS REDUCTION MODEL

INTERIOR

ROSETTE NUMBER	EPSILON A MICRO M/M	EPSILON B MICRO M/M	EPSILON C MICRO M/M	EPSILON 1 MICRO M/M	EPSILON 2 MICRO M/M	SIGMA 1*RO*RO*PI/P DIMENSIONLESS	SIGMA 2*RO*RO*PI/P DIMENSIONLESS
1	26.40	-10.60	-42.00	26.51	-42.11	5.990	-14.741
2	38.00	-20.00	-74.00	38.04	-74.04	6.829	-27.025
3	59.80	-12.20	-89.60	59.85	-89.65	14.221	-30.939
4	201.00	208.60	205.60	209.08	197.52	115.796	112.306
5	111.20	-1.40	-80.40	112.66	-81.86	38.020	-20.741

EXTERIOR

ROSETTE NUMBER	EPSILON A MICRO M/M	EPSILON B MICRO M/M	EPSILON C MICRO M/M	EPSILON 1 MICRO M/M	EPSILON 2 MICRO M/M	SIGMA 1*RO*RO*PI/P DIMENSIONLESS	SIGMA 2*RO*RO*PI/P DIMENSIONLESS
1	-2.00	7.00	14.40	14.44	-2.04	5.967	0.989
2	-24.60	-47.80	-90.40	-23.20	-91.80	-21.896	-42.619
3	-7.00	-31.40	-41.20	-5.51	-42.69	-7.904	-19.137

TABLE 4b

DATA, PRINCIPAL STRAINS, AND DIMENSIONLESS PRINCIPAL STRESS COEFFICIENTS FOR A 6.670 N (1.500 LB) LOAD AT LOAD LOCATION 2 ON THE 60 PERCENT MASS REDUCTION MODEL

INTERIOR

ROSETTE NUMBER	EPSILON A MICRO M/M	EPSILON B MICRO M/M	EPSILON C MICRO M/M	EPSILON 1 MICRO M/M	EPSILON 2 MICRO M/M	SIGMA 1*RO*RO*PI/P DIMENSIONLESS	SIGMA 2*RO*RO*PI/P DIMENSIONLESS
1	69.00	-7.00	-90.20	69.08	-90.28	18.123	-30.016
2	202.60	223.20	212.60	223.98	191.22	121.412	111.515
3	126.60	31.20	-68.20	126.62	-68.22	45.810	-13.047
4	49.00	-24.20	-84.40	49.32	-84.72	10.314	-30.174
5	27.40	-14.40	-47.40	27.66	-47.66	5.766	-16.986

EXTERIOR

ROSETTE NUMBER	EPSILON A MICRO M/M	EPSILON B MICRO M/M	EPSILON C MICRO M/M	EPSILON 1 MICRO M/M	EPSILON 2 MICRO M/M	SIGMA 1*RO*RO*PI/P DIMENSIONLESS	SIGMA 2*RO*RO*PI/P DIMENSIONLESS
1	-40.40	-57.40	-120.20	-34.30	-126.30	-31.151	-58.945
2	-19.20	-45.20	-51.40	-16.40	-54.20	-14.094	-25.513
3	-5.00	7.00	17.20	17.24	-5.04	6.786	0.058

TABLE 4c

DATA, PRINCIPAL STRAINS, AND DIMENSIONLESS PRINCIPAL STRESS COEFFICIENTS FOR A 6,670 N (1,500 LB) LOAD AT LOAD LOCATION 3 ON THE 60 PERCENT MASS REDUCTION MODEL

INTERIOR

ROSETTE NUMBER	EPSILON A MICRO M/M	EPSILON B MICRO M/M	EPSILON C MICRO M/M	EPSILON 1 MICRO M/M	EPSILON 2 MICRO M/M	SIGMA 1*RO*RO*PI/P DIMENSIONLESS	SIGMA 2*RO*RO*PI/P DIMENSIONLESS
1	165.20	63.80	-17.00	165.78	-17.58	69.264	13.876
2	62.60	-21.40	-97.20	62.71	-97.31	14.462	-33.873
3	36.40	2.40	-60.20	38.47	-62.27	8.540	-21.892
4	23.00	-5.60	-30.40	23.07	-30.47	6.010	-10.162
5	17.00	-0.80	-15.80	17.06	-15.86	5.309	-4.635

EXTERIOR

ROSETTE NUMBER	EPSILON A MICRO M/M	EPSILON B MICRO M/M	EPSILON C MICRO M/M	EPSILON 1 MICRO M/M	EPSILON 2 MICRO M/M	SIGMA 1*RO*RO*PI/P DIMENSIONLESS	SIGMA 2*RO*RO*PI/P DIMENSIONLESS
1	-35.00	-59.00	-68.40	-33.47	-69.93	-23.498	-34.509
2	-0.20	8.40	18.20	18.22	-0.22	7.834	2.264
3	-11.20	1.00	13.20	13.20	-11.20	4.246	-3.124

TABLE 4d

DATA, PRINCIPAL STRAINS, AND DIMENSIONLESS PRINCIPAL STRESS COEFFICIENTS FOR A 6,670 N (1,500 LB) LOAD AT LOAD LOCATION 4 ON THE 60 PERCENT MASS REDUCTION MODEL

INTERIOR

ROSETTE NUMBER	EPSILON A MICRO M/M	EPSILON B MICRO M/M	EPSILON C MICRO M/M	EPSILON 1 MICRO M/M	EPSILON 2 MICRO M/M	SIGMA 1*RO*RO*PI/P DIMENSIONLESS	SIGMA 2*RO*RO*PI/P DIMENSIONLESS
1	38.40	-9.20	-61.60	38.46	-61.66	8.614	-21.629
2	29.20	0.00	-34.20	29.30	-34.30	8.203	-11.008
3	18.40	5.40	-16.60	18.97	-17.17	5.963	-4.953
4	15.40	-0.20	-11.00	15.62	-11.22	5.287	-2.819
5	14.00	1.20	-13.00	14.02	-13.02	4.364	-3.803

EXTERIOR

ROSETTE NUMBER	EPSILON A MICRO M/M	EPSILON B MICRO M/M	EPSILON C MICRO M/M	EPSILON 1 MICRO M/M	EPSILON 2 MICRO M/M	SIGMA 1*RO*RO*PI/P DIMENSIONLESS	SIGMA 2*RO*RO*PI/P DIMENSIONLESS
1	-1.60	6.20	18.20	18.42	-1.82	7.713	1.599
2	-1.40	2.40	15.20	16.34	-2.54	6.723	1.019
3	-11.20	0.80	13.40	13.40	-11.20	4.334	-3.100

TABLE 5

DIMENSIONLESS PRINCIPAL STRESS

COEFFICIENTS CALCULATED FROM THEORETICAL SOLUTION

FOR INTERIOR SURFACE STRESSES

$$K = \sigma : P/\pi R_o^2$$

Mass Reduction	40%		50%		60%	
θ	K_1	K_2	K_1	K_2	K_1	K_2
0	-43.12	-43.12	-75.95	-75.95	-142.82	-142.82
10	- 9.64	-24.89	-4.81	-34.20	7.07	- 46.99
20	10.70	- 9.67	19.01	-11.52	33.20	- 14.25
30	13.32	- 4.60	19.84	- 5.47	30.04	- 7.23
40	11.80	- 3.09	15.94	- 4.01	21.26	- 6.08
50	9.30	- 2.79	11.37	- 3.84	13.38	- 5.79
60	6.90	- 2.87	7.61	- 3.91	8.03	- 5.48
70	5.06	- 3.02	5.04	- 3.94	4.97	- 5.13
80	3.94	- 3.12	3.59	- 3.92	3.51	- 4.70
90	3.57	- 3.15	3.13	- 3.89	3.09	- 4.48

NASA-Langley, 1974 E-7976

"The aeronautical and space activities of the United States shall be conducted so as to contribute . . . to the expansion of human knowledge of phenomena in the atmosphere and space. The Administration shall provide for the widest practicable and appropriate dissemination of information concerning its activities and the results thereof."

—NATIONAL AERONAUTICS AND SPACE ACT OF 1958

NASA SCIENTIFIC AND TECHNICAL PUBLICATIONS

TECHNICAL REPORTS: Scientific and technical information considered important, complete, and a lasting contribution to existing knowledge.

TECHNICAL NOTES: Information less broad in scope but nevertheless of importance as a contribution to existing knowledge.

TECHNICAL MEMORANDUMS: Information receiving limited distribution because of preliminary data, security classification, or other reasons. Also includes conference proceedings with either limited or unlimited distribution.

CONTRACTOR REPORTS: Scientific and technical information generated under a NASA contract or grant and considered an important contribution to existing knowledge.

TECHNICAL TRANSLATIONS: Information published in a foreign language considered to merit NASA distribution in English.

SPECIAL PUBLICATIONS: Information derived from or of value to NASA activities. Publications include final reports of major projects, monographs, data compilations, handbooks, sourcebooks, and special bibliographies.

TECHNOLOGY UTILIZATION PUBLICATIONS: Information on technology used by NASA that may be of particular interest in commercial and other non-aerospace applications. Publications include Tech Briefs, Technology Utilization Reports and Technology Surveys.

Details on the availability of these publications may be obtained from:

SCIENTIFIC AND TECHNICAL INFORMATION OFFICE

NATIONAL AERONAUTICS AND SPACE ADMINISTRATION

Washington, D.C. 20546